Inorg. Chem. **2005**, *44*, 4506–4514

cis-Dioxomolybdenum(VI) and Oxo(phosphine oxide)molybdenum(IV) Complexes: Steric and Electronic Fine-Tuning of *cis*-$[MoOS]^{2+}$ Precursors

Christian J. Doonan, Andrew J. Millar, David J. Nielsen, and Charles G. Young*

School of Chemistry, University of Melbourne, Victoria 3010, Australia

Received December 23, 2004

The complexes *cis*-$Tp^{iPr}Mo^{VI}O_2(OAr)$ (Tp^{iPr} = hydrotris(3-isopropylpyrazol-1-yl)borate, ^-OAr = phenolate or naphtholate derivative) are formed upon metathesis of $Tp^{iPr}MoO_2Cl$ and $HOAr/NEt_3$ in dichloromethane. The orange, diamagnetic dioxo-Mo(VI) complexes exhibit strong $\nu(MoO_2)$ IR bands at ca. 930 and 905 cm^{-1} and NMR spectra indicative of C_s symmetry. They undergo electrochemically reversible, one-electron reductions at potentials in the range –0.714 to –0.855 V vs SCE (in MeCN) and react with PEt_3 to produce $Tp^{iPr}Mo^{IV}O(OAr)(OPEt_3)$. The green, diamagnetic oxo-Mo(IV) complexes display a single $\nu(MoO)$ IR band at ca. 950 cm^{-1} and exhibit NMR spectra indicative of C_1 symmetry. The crystal structures of eight dioxo-Mo(VI) complexes have been determined to assess the degree of frontal (O_3-donor face) steric congestion at the Mo center, to identify complexes amenable to conversion into *monomeric* oxosulfido-Mo(VI) derivatives. The complexes display distorted octahedral geometries, with a cis arrangement of terminal oxo ligands, with $d(Mo{=}O)_{av}$ = 1.694 Å and $\angle(MoO_2)_{av}$ = 103.4°. Maximal frontal steric congestion is observed in the 2-phenolate derivatives, and these are identified as precursors for *strictly monomeric* (solid and solution state) oxosulfido-Mo(VI) counterparts.

Introduction

cis-Dioxo complexes dominate the chemistry of Mo(VI), and their prevalence, ease of synthesis, and chemical attributes have led to their exploitation as oxidation catalysts, models for enzymes and surface oxides, sensors, and drug targets for iron overload, thalassemia, and heart dysfunction in diabetics.[1,2] Coordination numbers of 4−6 are known, but six-coordinate, distorted octahedral species are most common; complexes of this type form with a wide range of halide and pure or mixed C-, N-, O-, and S-donor ligands.[1,2] The predilection of dioxo-Mo(VI) complexes for oxygen atom transfer (OAT) reactions makes them potential oxidation catalysts and relevant models for certain molybdenum enzymes, including sulfite oxidase and nitrate reductase.[3−6] Biomimetic OAT systems have been extensively reviewed.[6−9]

Tris(pyrazolyl)borate ligands[10] have played a significant role in the development of models for molybdenum enzymes, and a catalytic system that combines OAT and coupled electron−proton transfer (CEPT) reactions has been developed.[7] Most work in this area has focused on complexes of the hydrotris(3,5-dimethylpyrazol-1-yl)borate ligand (Tp*),[7] but complexes containing hydrotris(3-isopropylpyrazol-1-yl)-borate (Tp^{iPr}) are now attracting attention. Dioxo-Mo(VI)

* Author to whom correspondence should be addressed. E-mail: cgyoung@unimelb.edu.au.

(1) Stiefel, E. I. In *Comprehensive Coordination Chemistry*; Wilkinson, G., Gillard, R. D., McCleverty, J. A. Eds.; Pergamon: Oxford, U.K., 1987; Chapter 36.5, pp 1375−1420.
(2) Young, C. G. In *Comprehensive Coordination Chemistry II*; McCleverty, J. A., Meyer, T. J., Eds.; Elsevier Pergamon: Amsterdam, 2004; Chapter 4.7, pp 415−527.
(3) Pilato, R. S.; Stiefel, E. I. In *Bioinorganic Catalysis*; Reedijk, J., Bouwman, E., Eds.; Marcel Dekker: New York, 1999; pp 81−152.
(4) Sigel, A., Sigel, H., Eds. *Metal Ions in Biological Systems*; Marcel Dekker: New York, 2002; Vol. 39.
(5) Tunney, J. M.; McMaster, J.; Garner, C. D. In *Comprehensive Coordination Chemistry II*; McCleverty, J. A., Meyer, T. J., Eds.; Elsevier Pergamon: Amsterdam, 2004; Chapter 8.18, pp 459−477.
(6) Young, C. G. In *Encyclopedia of Inorganic Chemistry 2*; King, R. B., Scott, R. A., Eds.; Wiley: Chichester, U.K., 2005, in press.
(7) Young, C. G. In *Biomimetic Oxidations Catalyzed by Transition Metal Complexes*; Meunier, B., Ed.; Imperial College Press: London, 2000; pp 415−459.
(8) McMaster, J.; Tunney, J. M.; Garner, C. D. *Prog. Inorg. Chem.* **2004**, *52*, 539−583.
(9) Enemark, J. H.; Cooney, J. J. A.; Wang, J.-J.; Holm, R. H. *Chem. Rev.* **2004**, *104*, 1175−1200.
(10) Trofimenko, S. *Scorpionates: The Coordination Chemistry of Polypyrazolylborate Ligands*; Imperial College Press: London, 1999.

10.1021/ic050052v CCC: $30.25
Published on Web 05/24/2005

complexes such as Tp$^{i\mathrm{Pr}}$MoO$_2$X (X = OMe, phenolates, S^{n}Bu, S^{s}Bu) and facets of their atom transfer chemistry have been reported.[11−13] The OAT and catalytic activity of Tp^{x}MoO$_2$X (Tp^x = tris(pyrazolyl)borate derivative) complexes are correlated with their Mo^{VI}/Mo^V redox potentials; these span a 700 mV range, in the order (X) OR$^-$ < SR$^-$ < OPh$^-$ < SPh$^-$ < halide < SCN$^-$.[11,13] Reduction potentials are also influenced by the pyrazolylborate ligand, with a 240 mV variation in the order Tp* < Tp$^{i\mathrm{Pr}}$ < Tz* (Tz* = hydrotris(3,5-dimethyl-1,2,4-triazol-1-yl)borate).[11] Additional influences on the primary and secondary (e.g., comproportionation, internal redox, dinucleation) reactions of Tp^{x}MoO$_2$X complexes,[7] especially the steric influence of the coligand, X, have not been fully assessed.

Our interest in fine-tuning the electronic and steric properties of Tp$^{i\mathrm{Pr}}$Mo complexes stems inter alia from a desire to prepare *monomeric* oxosulfido-Mo(VI) complexes as models for molybdenum hydroxylases.[4,5,14] We have shown that Tp$^{i\mathrm{Pr}}$MoO$_2$X complexes react with tertiary phosphines to produce Tp$^{i\mathrm{Pr}}$MoOX(OPR$_3$)[15] and that Tp$^{i\mathrm{Pr}}$MoO(OPh)(OPEt$_3$) reacts with propylene sulfide to produce the oxosulfido-Mo(VI) complex, Tp$^{i\mathrm{Pr}}$MoOS(OPh).[16] The isolation of monomeric Tp$^{i\mathrm{Pr}}$MoOS(OPh) was thwarted by the crystallization of the μ-disulfido-Mo(V) dimer, [Tp$^{i\mathrm{Pr}}$MoO(OPh)]$_2$(μ-S$_2$). The isolation of *strictly monomeric* (solid and solution state) Tp$^{i\mathrm{Pr}}$MoOS(OPh) derivatives would be enhanced by (i) reducing the likelihood of Mo═S redox, by operating at marginally more negative reduction potentials than in the phenolate system,[17] and (ii) preventing close approach of the metal centers by increasing the frontal steric congestion, i.e., at the O$_2$S-donor ligand face, opposite the *fac*-Tp$^{i\mathrm{Pr}}$ ligand, in the oxosulfido-Mo(VI) complex (and by inference its dioxo-Mo(VI) and oxo-Mo(IV) precursors).

We report here the synthesis and characterization of new dioxo-Mo(VI) complexes, Tp$^{i\mathrm{Pr}}$MoO$_2$(OAr) (OAr = phenolate or naphtholate derivative), and their oxo(phosphine oxide)-Mo(IV) derivatives, Tp$^{i\mathrm{Pr}}$MoO(OAr)(OPEt$_3$). Electrochemical and crystallographic studies, undertaken to identify likely precursors for strictly *monomeric* oxosulfido-Mo(VI) complexes, are also reported. The phenolate and naphtholate coligands included in this study and the numbering scheme for the dioxo-Mo(VI) complexes are given in Chart 1. The outcomes of reactions aimed at producing oxosulfido-Mo(VI) derivatives, alluded to herein, are described in other publications.[18]

Chart 1. $^-$OAr Ligands[a]

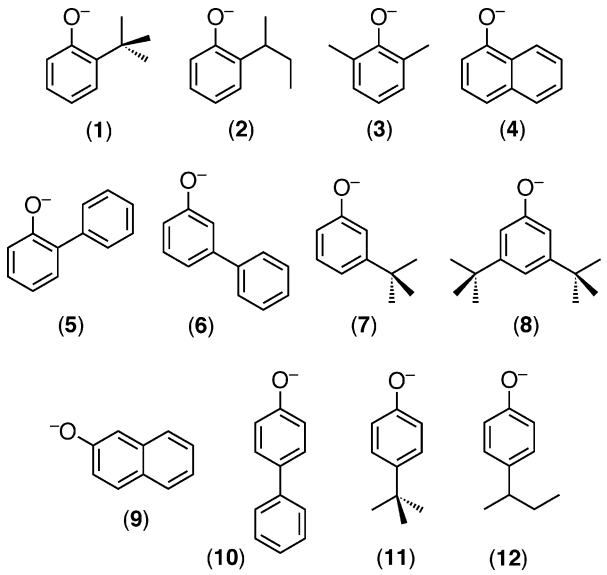

[a] Numbers refer to the corresponding Tp$^{i\mathrm{Pr}}$MoO$_2$(OAr) complex.

Experimental Section

Materials and Methods. All reactions were performed under an atmosphere of dinitrogen using standard Schlenk techniques and dried, deoxygenated solvents. Samples of Tp$^{i\mathrm{Pr}}$MoO$_2$Cl were prepared by a modification of the literature method,[11] the starting materials being dried in vacuo at 50 °C for 6 h immediately prior to use. Phenols were obtained from commercial sources and were used as received, with the exception of 3-phenylphenol, which was twice recrystallized from boiling hexane to reduce the level of 4-phenylphenol contamination. Triethylphosphine was sourced from Fluka Chemical Co and was used as received. The complexes **2**, **7**, and **8** were prepared according to literature methods.[13]

Infrared spectra were recorded on a Biorad FTS 165 FTIR spectrophotometer as pressed KBr disks. Proton NMR spectra were obtained using a Varian FT UnityPlus 400 MHz spectrometer. The spectra of Tp$^{i\mathrm{Pr}}$MoO$_2$(OAr) complexes were recorded in CDCl$_3$ and referenced to residual CHCl$_3$ (δ 7.26), while those of Tp$^{i\mathrm{Pr}}$MoO(OAr)(OPEt$_3$) were recorded in C$_6$D$_6$ and referenced to TMS (δ 0.00); samples of the latter were prepared under anaerobic conditions by employing sealed tubes. Mass spectra were recorded on a Bruker BioApex 47e FTMS fitted with an Analytica electrospray source operating with capillary voltages between 30 and 120 V; samples of Tp$^{i\mathrm{Pr}}$MoO$_2$(OAr) and Tp$^{i\mathrm{Pr}}$MoO(OAr)(OPEt$_3$) were run in CH$_2$Cl$_2$ and MeCN, respectively. Electrochemical measurements were performed using a Cypress Electrochemical System II configured with a 3 mm glassy-carbon working electrode, a platinum auxiliary electrode, and a reference electrode consisting of an Ag/AgNO$_3$ (0.01 M in MeCN) electrode incorporated into a salt bridge containing supporting electrolyte (to minimize Ag$^+$ leakage). Sample solutions were prepared in acetonitrile/0.1 M N^{n}Bu$_4$BF$_4$ (or in the case of **1**, dichloromethane/0.2 M N^{n}Bu$_4$PF$_6$). Potentials were referenced against internal ferrocene (Fc) and are

(11) Xiao, Z.; Bruck, M. A.; Doyle, C.; Enemark, J. H.; Grittini, C.; Gable, R. W.; Wedd, A. G.; Young, C. G. *Inorg. Chem.* **1995**, *34*, 5950−5962. (Erratum: *Inorg. Chem.* **1996**, *35*, 5752.)
(12) Xiao, Z.; Gable, R. W.; Wedd, A. G.; Young, C. G. *J. Am. Chem. Soc.* **1996**, *118*, 2912−2921.
(13) Millar, A. J.; Doonan, C. J.; Laughlin, L. J.; Tiekink, E. R. T.; Young, C. G. *Inorg. Chim. Acta* **2002**, *337*, 393−406.
(14) Young, C. G. *J. Biol. Inorg. Chem.* **1997**, *2*, 810−816.
(15) (a) Smith, P. D.; Millar, A. J.; Young, C. G.; Ghosh, A.; Basu, P. *J. Am. Chem. Soc.* **2000**, *122*, 9298−9299. (b) Millar, A. J.; Doonan, C. J.; Smith, P. D.; Nemykin, V. N.; Basu, P.; Young, C. G. *Chem.—Eur. J.* **2005**, *11*, 3255−3267. (c) Kail, B. W.; Pérez, L. M.; Zaric, S. D.; Millar, A. J.; Young, C. G.; Hall, M. B.; Basu. P. Submitted for publication.
(16) Smith, P. D.; Slizys, D. A.; George, G. N.; Young, C. G. *J. Am. Chem. Soc.* **2000**, *122*, 2946−2947.
(17) Eagle, A. A.; Tiekink, E. R. T.; George, G. N.; Young, C. G. *Inorg. Chem.* **2001**, *40*, 4563−4573.
(18) (a) Doonan, C. J. Ph.D. Dissertation, University of Melbourne, Parkville, Australia, 2004. (b) Doonan, C. J.; Nielsen, D. J.; Smith, P. D.; White, J. M.; George, G. N.; Harris, H.; Young, C. G. Manuscript in preparation.

reported relative to the saturated calomel electrode ($E_{1/2}(Fc^+/Fc) = 0.460$ V vs SCE[19]). Microanalyses were performed by Atlantic Microlabs, Norcross, GA.

Syntheses. Tp^{iPr}MoO$_2$(OAr). The procedure below was adopted for all Tp^{iPr}MoO$_2$(OAr) complexes: A 100 mL Schlenk flask was charged with Tp^{iPr}MoO$_2$Cl (1.00 g, 1.99 mmol) and a 4-fold molar excess of solid HOAr (where HOAr was a liquid, it was added just before triethylamine (vide infra)). Dichloromethane (30 mL) was added to produce a yellow solution, followed by a 7-fold molar excess of triethylamine. The resulting solution was stirred for 24 h (or 4−5 days for **1**) and then evaporated to dryness. The residue was chromatographed on silica gel by employing 3:2 CH_2Cl_2−hexane as eluent. The main orange fraction was collected and reduced to dryness, and the crude product was recrystallized from dichloromethane−hexane to yield orange crystals. Yields ranged from 40 to 80%.

Characterization data are summarized in Table 1. Full listings of IR bands may be found in the Supporting Information.

Tp^{iPr}MoO(OAr)(OPEt$_3$). The procedure below was adopted for all Tp^{iPr}MoO(OAr)(OPEt$_3$) complexes: A solution or suspension of Tp^{iPr}MoO$_2$(OAr) (1.00 g) in acetonitrile (30 mL) was treated with a 1.5 molar excess of PEt$_3$ and stirred overnight (or 4−5 days in the case of Tp^{iPr}MoO(OC$_6$H$_4$^{t}Bu-2)(OPEt$_3$)). The resulting dark green solution was evaporated to dryness and the residue triturated with hexane (15 mL); this process was repeated to yield a green microcrystalline powder that was isolated by filtration and washed with cold hexane. Yields ranged from 60 to 85%.

Characterization data are summarized in Table 1. Full listings of IR bands may be found in the Supporting Information.

X-ray Crystallography. All crystals were grown by diffusion of methanol or hexane into dichloromethane solutions of the complexes. Crystallographic data are summarized in Tables 2 and 3.

Diffraction data were collected on a Bruker CCD area detector at 293 K using Mo Kα radiation (0.710 73 Å). Data were collected to $2\theta = 55°$ for each structure. Cell parameters were acquired using the SMART software package, and data reduction was performed with SAINT. Structures were solved by direct methods (SHELXS-97)[20] and refined using full-matrix least squares on F^2 (SHELXL-97).[21] Generally, non-H atoms were refined anisotropically and H atoms were included in their calculated positions using the riding model. For **2**, analysis of difference maps indicated that the *sec*-butyl group was disordered. The group was modeled over two positions with one atom (C(9)) common to both positions of the *sec*-butyl group. The sum of the site occupancies of the two orientations was constrained to equal one, and all atoms were refined isotropically. Molecular diagrams were generated using ORTEP 3.[22] Selected distances and angles are presented in Tables 4 and 5, respectively.

Results and Discussion

***cis*-Dioxo-Mo(VI) Complexes.** Orange *cis*-Tp^{iPr}MoO$_2$(OAr) were synthesized according to eq 1. Reaction times depended on the phenolate ligands; those containing bulky 2- or 2,6-alkyl groups required long reaction times, while

Table 1. Selected Characterization Data

	IR spectral data (KBr, cm^{-1})			^{1}H NMR spectral data, δ (mult, no. of H)				
compd (Ar, no.)	ν(BH)	ν(MoO)	ν(PO)	Tp^{iPr} methyl[a]	Tp^{iPr} methine[b]	Tp^{iPr} ring[c]	OPR$_3$[d]	OAr[e]
				Tp^{iPr}MoO$_2$(OAr) Complexes				
C$_6$H$_4$^{t}Bu-2 (**1**)	2480	931, 903		0.45, 1.08, 1.30	3.50 (2H), 4.51	6.00 (2H), 6.17, 7.64 (2H), 7.65		1.46 (9H), 4.64 (d), 6.45 (t), 6.80 (t), 7.19 (t) (each 1H)
C$_6$H$_3$Me$_2$-2,6 (**3**)	2487	935, 907		0.79, 1.10, 1.26	3.50 (2H), 4.42	6.05 (2H), 6.09, 7.57, 7.58 (2H)		0.91 (s, 3H), 2.55 (s, 3H), 6.6−7.0 (m, 3H)
C$_{10}$H$_7$-1 (**4**)	2505	928, 905		0.57, 1.02, 1.30	3.36 (2H), 4.44	6.05 (2H), 6.17, 7.64 (2H), 7.66		7.25−7.88 (7H)
C$_6$H$_4$Ph-2 (**5**)	2502	937, 905		0.97, 1.12, 1.30	3.49 (2H), 4.39	6.08 (2H), 6.15, 7.62 (2H), 7.65		6.89−7.62 (9H)
C$_6$H$_4$Ph-3 (**6**)	2494	931, 900		0.93, 1.11, 1.29	3.52 (2H), 4.39	6.07 (2H), 6.15, 7.61 (2H), 7.64		6.96 (t, 1H), 6.81 (d of d, 1H), 7.17 (d, 1H), 7.30 (t, 1H), 7.32 (t, 1H), 7.41 (t, 2H), 7.52 (d, 2H)
C$_{10}$H$_7$-2 (**9**)	2545	924, 903		0.92, 1.07, 1.31	3.47 (2H), 4.42	6.08 (2H), 6.16, 7.63 (2H), 7.65		7.02−7.80 (m, 7H)
C$_6$H$_4$Ph-4 (**10**)	2584	923, 902		0.97, 1.12, 1.30	3.50 (2H), 4.40	6.09 (2H), 6.15, 7.62 (2H), 7.65		6.90 (d, 2H), 7.28 (t, 1H), 7.42 (t, 2H), 7.50 (d, 2H), 7.58 (d, 2H)
C$_6$H$_4$^{t}Bu-4 (**11**)	2580	927, 904		0.92, 1.09, 1.28	3.49 (2H), 4.40	6.06 (2H), 6.12, 7.59 (2H), 7.61		1.28 (s, 9H), 6.74 (d, 2H), 7.22 (d, 2H)
C$_6$H$_4$^{s}Bu-4 (**12**)	2507	930, 898		0.91, 1.10, 1.28	3.49 (2H), 4.40	6.06 (2H), 6.13, 7.60 (2H), 7.62		0.78 (t, 3H), 1.20 (d, 3H), 1.55 (quartet, 2H), 2.53 (septet, 1H), 6.71 (t) and 7.01 (t) (each 2H)
				Tp^{iPr}MoO(OAr)(OPEt$_3$) Complexes				
C$_6$H$_4$^{t}Bu-2	2488, 2477	948	1122	0.44, 1.04, 1.12, 1.15, 1.31, 1.77	2.44, 4.22, 4.28	5.90, 5.94, 6.01, 7.33, 7.41, 7.67	0.84, 1.53, 2.00	1.63 (9H), 5.59 (3H), 6.71 (1H)
C$_{10}$H$_7$-1	2477, 2446	948	1102	−0.05, 0.86, 0.92, 1.13, 1.26, 1.68	2.50, 4.12, 4.44	5.80, 5.90, 6.01, 7.39, 7.43, 7.66	1.02, 1.63, 2.19	5.89−8.34 (m, 7H)
C$_6$H$_4$Ph-2	2476, 2445	950	1098	0.60, 0.98, 1.07, 1.19, 1.24, 1.31	3.04, 4.02, 4.26	5.88, 5.97, 6.02, 7.36, 7.45, 7.71	0.74, 1.42, 1.70	5.18−7.68 (m, 9H)
C$_6$H$_4$Ph-3	2477, 2451	949	1087	0.60, 1.00, 1.07, 1.20, 1.25, 1.68	2.73, 4.17, 4.41	5.82, 5.92, 6.01, 7.39, 7.44, 7.72	0.94, 1.71, 1.96	6.43−7.45 (m, 9H)
C$_{10}$H$_7$-2	2478, 2447	946	1101	0.25, 0.92, 0.96, 1.13, 1.27, 1.69	2.66, 4.14, 4.40	5.84, 5.88, 6.01, 7.42, 7.46, 7.73	0.98, 1.70, 1.96	6.44−7.62 (m, 7H)
C$_6$H$_4$Ph-4	2480, 2449	945	1103	0.61, 1.01, 1.10, 1.19, 1.24, 1.68	2.66, 4.13, 4.40	5.88, 5.97, 6.00, 7.37, 7.43, 7.73	0.88, 1.66, 2.22	6.33−7.49 (m, 9H)
C$_6$H$_4$^{t}Bu-4	2480, 2452	950	1083	0.49, 0.94, 1.06, 1.13, 1.20, 1.63	2.55, 4.17, 4.40	5.83, 5.92, 5.94, 7.33, 7.38, 7.67	0.95, 1.64, 1.93	1.18 (9H), 6.22 (2H), 7.00 (2H)
C$_6$H$_4$^{s}Bu-4	2473, 2446	950	1082	0.60, 0.9−1.3,[f] 1.70	2.40, 4.19, 4.44	5.88, 5.97, 6.00, 7.37, 7.43, 7.73	~1.0,[f] 1.66, 2.00	0.84 (t, 3H), 1.20 (d, 3H),[g] 1.50 (m, 2H), 2.66 (m, 1H), 6.25 (d, 2H), 6.86 (d, 2H)

[a] All doublet resonances integrating for 6H (dioxo complexes) or 3H (OPEt$_3$ complexes). [b] All septet resonances integrating for 1H each unless indicated. [c] All doublet resonances integrating for 1H each unless indicated. [d] For OPEt$_3$ complexes, most shielded resonance is a doublet of triplets (9H); the other two are doublets of quartets (3H each), with $^3J_{HP} \sim 17$ Hz, $^2J_{HP} \sim 15$ Hz, $^2J_{HH} \sim 15$ Hz, and $^3J_{HH} \sim 8$ Hz. [e] Peaks obscured by overlapping resonances.

(19) Connelly, N. G.; Gieger, W. E. *Chem. Rev.* **1996**, *96*, 877−910.
(20) Sheldrick, G. M. *SHELXS-97 Program for Crystal Structure Solution*; University of Göttingen: Göttingen, Germany, 1997.
(21) Sheldrick, G. M. *SHELXL-97 Program for Crystal Structure Refinement*; University of Göttingen: Göttingen, Germany, 1997.
(22) Farrugia, L. J. *J. Appl. Crystallogr.* **1997**, *30*, 565.

Table 2. Crystallographic Data (Monoclinic Units Cells)

	1	4	7	9
formula	$C_{28}H_{41}BMoN_6O_3$	$C_{28}H_{35}BMoN_6O_3$	$C_{28}H_{41}BMoN_6O_3$	$C_{28}H_{35}BMoN_6O_3$
fw	616.42	610.37	616.42	610.37
space group	$P2_1/c$	$P2_1/n$	$P2_1/c$	Pn
a, Å	14.6176(12)	11.2017(8)	8.8614(13)	12.6654(10)
b, Å	11.1221(10)	15.8302(12)	36.061(5)	7.6780(6)
c, Å	19.5013(17)	16.8147(12)	10.1029(15)	15.3752(13)
β, deg	100.283(2)	100.139(1)	96.254(3)	99.593(2)
V, Å^3	3119.6(5)	2935.1(4)	3209.2(8)	1474.3(2)
Z	4	4	4	2
ρ_{calcd} (g/cm^3)	1.312	1.381	1.276	1.375
μ (cm^{-1})	4.58	4.86	4.45	4.84
R_1[a]	0.0493	0.0468	0.0491	0.0398
wR_2[b]	0.0629	0.0981	0.0977	0.0779

[a] $R_1 = \Sigma||F_o| - |F_c||/\Sigma|F_o|$. [b] $wR_2 = \{[\Sigma w(F_o^2 - F_c^2)^2/\Sigma(w|F_o^2|)^2]\}^{1/2}$.

Table 3. Crystallographic Data (Orthorhombic Unit Cells)

	2	3	8	**10**[a]
formula	$C_{28}H_{41}BMoN_6O_3$	$C_{26}H_{37}BMoN_6O_3$	$C_{32}H_{49}BMoN_6O_3$	$C_{30.5}H_{38}BClMoN_6O_3$
fw	616.42	588.37	672.52	677.86
space group	*Pbca*	*Pbca*	$Pna2_1$	*Pbcn*
a, Å	8.2162(6)	10.800(4)	16.929(4)	44.685(3)
b, Å	19.5964(14)	17.992(6)	17.526(5)	9.5365(7)
c, Å	38.418(3)	29.635(10)	12.051(3)	15.4123(11)
V, Å^3	6185.6(8)	5759(3)	3575.6(16)	6567.8(8)
Z	8	8	4	8
ρ_{calcd} (g/cm^3)	1.324	1.357	1.249	1.371
μ (cm^{-1})	4.17	4.92	4.05	5.21
R_1[b]	0.0651	0.0815	0.0379	0.0571
wR_2[c]	0.1458	0.1561	0.0972	0.1463

[a] For dichloromethane hemisolvate. [b] $R_1 = \Sigma||F_o| - |F_c||/\Sigma|F_o|$. [c] $wR_2 = \{[\Sigma w(F_o^2 - F_c^2)^2/\Sigma(w|F_o^2|)^2]\}^{1/2}$.

Table 4. Selected Bond Distances (Å)

dist	1	2	3	4	7	8	9	10
Mo−O(2)	1.685(3)	1.695(4)	1.696(4)	1.692(2)	1.692(3)	1.694(2)	1.697(3)	1.698(3)
Mo−O(3)	1.684(3)	1.700(3)	1.696(4)	1.692(2)	1.695(3)	1.697(2)	1.687(3)	1.702(3)
Mo−O(1)	1.886(3)	1.866(4)	1.891(3)	1.931(2)	1.898(3)	1.909(2)	1.910(3)	1.905(3)
O(1)−C_{OAr}	1.356(5)	1.376(6)	1.351(6)	1.349(4)	1.361(6)	1.358(4)	1.373(6)	1.352(5)
Mo−N(11)	2.177(4)	2.202(4)	2.206(4)	2.201(2)	2.181(4)	2.205(3)	2.179(4)	2.180(3)
Mo−N(21)	2.320(4)	2.342(4)	2.325(4)	2.317(3)	2.328(4)	2.326(3)	2.317(4)	2.322(4)
Mo−N(31)	2.315(4)	2.339(4)	2.372(4)	2.351(3)	2.317(4)	2.346(3)	2.302(4)	2.311(3)

Table 5. Selected Angles (deg)

angle	1	2	3	4	7	8	9	10
O(2)−Mo−O(3)	103.76(14)	103.56(18)	103.73(19)	102.44(11)	103.92(16)	103.44(13)	103.13(15)	103.49(15)
O(2)−Mo−O(1)	101.22(15)	102.45(17)	100.72(17)	100.41(10)	101.37(15)	103.36(11)	99.91(15)	101.06(14)
O(3)−Mo−O(1)	100.83(14)	100.87(18)	103.27(18)	101.37(10)	102.09(16)	99.55(11)	101.36(15)	100.96(14)
N(21)−Mo−O(1)	87.24(13)	85.81(15)	84.84(15)	84.06(9)	86.62(14)	86.04(10)	84.75(14)	84.31(13)
N(31)−Mo−O(1)	85.98(14)	86.57(15)	86.87(15)	84.18(9)	86.03(14)	85.13(10)	85.33(14)	85.50(12)
N(11)−Mo−O(1)	161.39(14)	161.23(15)	159.86(16)	158.06(9)	160.75(15)	159.06(10)	159.70(14)	159.75(13)
N(11)−Mo−O(3)	90.38(15)	85.81(15)	84.84(15)	92.56(10)	89.75(16)	86.04(10)	91.76(16)	84.31(13)
N(11)−Mo−O(2)	90.31(14)	89.80(16)	90.15(19)	92.93(10)	90.22(14)	90.68(11)	91.98(15)	91.73(14)
N(21)−Mo−N(31)	78.72(13)	78.65(15)	79.19(15)	79.68(9)	78.85(14)	81.22(10)	80.34(14)	79.67(12)
N(21)−Mo−N(11)	78.32(14)	79.08(14)	78.55(16)	79.26(9)	79.01(14)	76.93(9)	80.34(14)	80.00(13)
N(31)−Mo−N(11)	79.79(14)	79.65(14)	78.94(15)	78.91(9)	78.85(14)	80.35(11)	78.70(14)	79.19(12)
N(21)−Mo−O(3)	87.80(14)	88.22(16)	88.98(18)	89.03(10)	86.15(15)	88.04(12)	87.68(15)	87.44(14)
N(21)−Mo−O(2)	163.93(14)	163.85(16)	163.13(17)	166.48(10)	165.32(16)	163.50(10)	167.00(15)	166.50(14)
N(31)−Mo−O(3)	164.64(15)	164.45(16)	165.37(18)	166.91(10)	163.07(15)	167.99(11)	165.83(15)	164.98(14)
N(31)−Mo−O(2)	88.18(14)	87.92(16)	86.43(17)	88.03(10)	88.75(15)	86.04(11)	87.81(14)	88.35(13)
Mo−O(1)−C_{OAr}	157.4(3)	161.5(3)	153.4(3)	131.5(2)	148.4(3)	144.01(19)	146.2(3)	150.6(3)

sterically demanding ligands such as 2,6-di-*tert*-butylphenolate failed to react with $Tp^{iPr}MoO_2Cl$. The air-stable complexes were isolated in 40−80% yield following column chromatography and recrystallization from dichloromethane−hexane. Correct microanalyses were obtained for all complexes (see Supporting Information).

$$Tp^{iPr}MoO_2Cl + HOAr + NEt_3 \rightarrow Tp^{iPr}MoO_2(OAr) + NEt_3HCl \quad (1)$$

Infrared spectra (Table 1) exhibited bands at ca. 930 and 905 cm^{-1}, which were assigned to the $\nu_s(MoO_2)$ and $\nu_{as}(MoO_2)$ modes, respectively, of the *cis*-dioxo-Mo(VI)

Table 6. Electrochemical Data for $Tp^{iPr}MoO_2(OAr)$ (by Ascending $E_{1/2}$)

compd (Ar, no.)	$E_{1/2}$ (V)	ΔE_{pp} (mV)	I_{pa}/I_{pc}
$C_6H_4{}^tBu$-2 (**1**)[a]	−1.045	236	0.84
$C_6H_3{}^tBu_2$-3,5 (**8**)[b]	−0.855	65	0.99
$C_6H_3Me_2$-2,6 (**3**)	−0.849	66	1.01
$C_6H_4{}^sBu$-2 (**2**)[b]	−0.844	77	0.93
$C_6H_4{}^tBu$-3 (**7**)[b]	−0.814	75	0.96
$C_6H_4{}^sBu$-4 (**12**)	−0.813	86	0.94
C_6H_4Ph-2 (**5**)	−0.809	71	0.97
$C_6H_4{}^tBu$-4 (**11**)	−0.800	70	1.01
Ph[c]	−0.780	72	1.02
C_6H_4Ph-4 (**10**)	−0.751	74	0.95
$C_{10}H_7$-1 (**4**)	−0.746	72	0.98
$C_{10}H_7$-2 (**9**)	−0.735	68	0.99
C_6H_4Ph-3 (**6**)	−0.714	82	0.96

[a] Measured in dichloromethane at 100 mV/s. [b] From ref 13. [c] From ref 11.

moiety; the positions and intensities of these bands are consistent with the literature.[2] Bands characteristic of the Tp^{iPr} (ν(BH) 2590−2480 cm^{-1}, ν(CN) 1507 cm^{-1}) and phenolate/naphtholate (ν(CO) ca. 1570 cm^{-1}, $\nu(CC)_{ring}$ 1260 cm^{-1}) ligands were also evident.[11,13]

NMR spectra (Table 1) were consistent with molecular C_s symmetry. Thus, the methyl groups of Tp^{iPr} gave rise to three doublets in the δ 0.45−1.31 region with an integration of 6:6:6, while the isopropyl and ring methine protons produced septet (δ 3.3−4.5) and doublet (δ 6.0−7.7) resonances, respectively, with characteristic 2:1 integrated intensities. Interestingly, the phenolate 6-H resonances of **1** (δ 4.64) and **2** (δ 5.03[13]) were shielded by ca. 2 ppm relative to those of the free ligand, as was one of the phenolate methyl resonances of **3** (1.64 ppm more shielded than its partner). A reduced but noticeable shielding of 0.5 ppm has also been reported for the 2-H proton of **7** relative to the free ligand.[13] These observations are consistent with the maintenance of the solid-state structure in solution, the shielded proton being positioned in the proximal cleft (ring shielding zones) of the Tp^{iPr} ligand.

Electrochemistry. The electrochemical properties of the dioxo-Mo(VI) complexes in acetonitrile were investigated by cyclic voltammetry, and results are summarized in Table 6. With the exception of **1**, all complexes exhibited a single, reversible, one-electron reduction in the potential range of −0.714 to −0.855 V; no other electrochemical processes were observed. Consistent with diffusion-controlled redox processes,[23] the $E_{1/2}$ values were independent of scan rates and peak current ratios were close to unity in all cases. The reduction potentials of the alkylphenolate derivatives were more negative than that of $Tp^{iPr}MoO_2(OPh)$, in the range previously associated with thiolate and alkoxide coligation; i.e., the incorporation of alkyl substituents on the phenolate stabilized the dioxo complexes relative to the corresponding anions.[11,13] This is expected to confer redox stability on accessible $Tp^{iPr}MoOS(OAr)$ derivatives, compared to $Tp^{iPr}MoOS(OPh)$. The reduction potentials of **6** and **10**, and the naphtholate complexes were slightly more positive than that of $Tp^{iPr}MoO_2(OPh)$ and the other phenolate derivatives. Complex **1** was insoluble in acetonitrile; in dichloromethane it exhibited a quasi-reversible reduction at −1.045 V. The electrochemical results are indicative of reduction to stable Mo(V) anions under the conditions of the experiments and are consistent with previous studies of related trispyrazolylborate complexes.[11,13]

Crystal Structures. The structures of **1**−**4** and **7**−**10** were determined by X-ray diffraction; ORTEP projections are shown in Figures 1−6, with selected bond distances and angles presented in Tables 4 and 5, respectively.

All the complexes exhibit six-coordinate, distorted octahedral geometries, with coordination spheres comprised of *facial* tridentate Tp^{iPr} and mutually cis monodentate phenolate/naphtholate and terminal oxo ligands. The Mo═O distances of 1.684(3)−1.702(3) Å and O═Mo═O angles of 102.44(11)−103.92(16)° are expected of *cis*-dioxo-Mo(VI) species.[2,24] These parameters are close to the values observed for $Tp^{iPr}MoO_2(OMe)$ (d(Mo═O) = 1.697(2) and 1.705(2) Å, ∠(O═Mo═O) = 103.78(8)°), the only other structurally characterized dioxo-Mo(VI) Tp^{iPr} complex.[11] The Mo−OAr and O−C bond distances fall in the ranges 1.866(4)−1.931(2) and 1.349(4)−1.376(6) Å, respectively. There is considerable variation in the observed Mo−O−C angles, in the range 131−162°, with complexes bearing sterically demanding 2-phenolates displaying the largest Mo−O−C angles (i.e., greater than 150°). Crystal packing influences are also likely to impact on the angle observed, but these are difficult to assess. The Mo−N distances are as expected, the two bonds trans to the oxo ligands being lengthened by ca. 0.14 Å compared to the third. The obtuse O−Mo−O angles and acute N−Mo−N angles observed are characteristic of Tp^xMoO_2X complexes and result from a displacement of the Mo atom toward the O_3-donor face and away from the N_3-donor face.[2,11] As a result the trans O−Mo−N angles, especially the ArO−Mo−N(11) angles of ca. 160°, deviate considerably from the ideal octahedral angle of 180° and the Mo atom sits slightly out of the equatorial plane defined by O(2), O(3), N(21), and N(31), toward the O(1) donor atom. The Tp^{iPr} isopropyl groups adopt conformations that project the methine proton toward the pseudoaxis through Mo and B.

The conformations of the phenolate/naphtholate coligands appear to be largely determined by intramolecular interactions, the bulky Tp^{iPr} isopropyl groups dictating the gross conformations of the sterically bulky coligands. The dioxo complexes fall into two broad categories depending on the degree of frontal (O_3-donor face) steric congestion from the coligands: (i) derivatives **1**−**4**, where there is significant frontal steric congestion; (ii) complexes **7**−**10**, where coligand substituents make a minimal contribution to frontal steric congestion.

In complexes **1** and **2** (Figure 1) the steric bulk of the 2-butyl groups prevents them from being accommodated in the proximal cleft of the Tp^{iPr} ligand; consequently, they project forward of the Mo−Tp^{iPr} unit, shielding the oxo

(23) Christensen, P. A.; Hamnett, A. *Techniques and Mechanisms in Electrochemistry*; Chapman and Hall: Oxford, U.K., 1994.

(24) Orpen, A. G.; Brammer, L.; Allen, F. H.; Kennard, O.; Watson, D. G.; Taylor, R. *J. Chem. Soc., Dalton Trans.* **1989**, S1−S83.

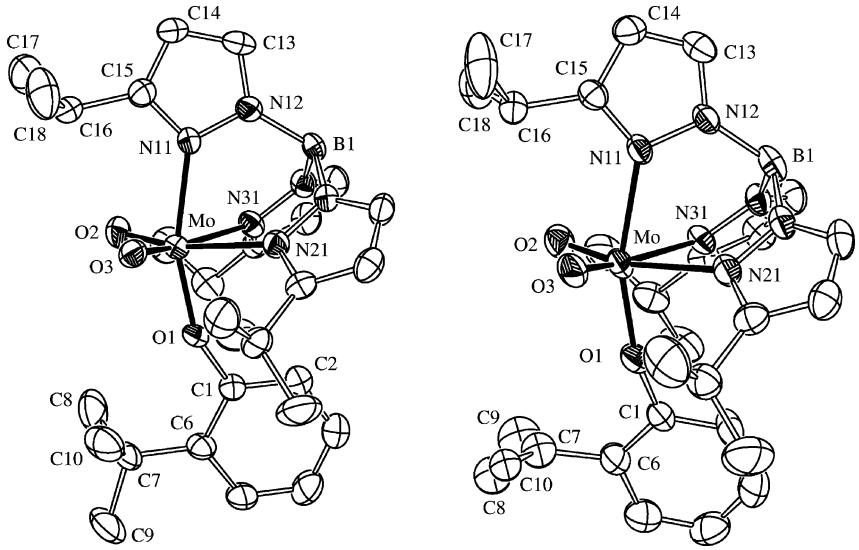

Figure 1. ORTEP projections of **1** (left) and **2** (right) drawn at 40% probability levels with hydrogen atoms removed. A single conformation of the disordered *sec*-butyl group of **2** is shown.

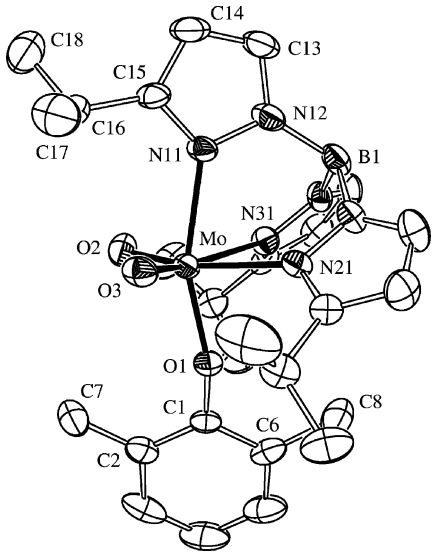

Figure 2. ORTEP projection of **3** drawn at the 40% probability level with hydrogen atoms removed.

ligands and metal center. In **1**, the phenolate ligand lies close to the pseudo-mirror plane (i.e., the plane containing Mo, B, and the N(11) pyrazole ring) of the complex, the planar arene ring making a small dihedral angle of 3.7° with the mirror plane. This is not the case with **2**, the arene ring making a dihedral angle of ca. 20.4° with the pseudo-mirror plane. The arene ring in **3** (Figure 2) is also inclined to the pseudo-mirror plane, the dihedral angle being 23.4°; one phenolate methyl group projects into the proximal Tp^{iPr} cleft, and the other away from the cleft and toward the O_3-donor face. The deviations of the coligands in **2** and **3** from the pseudo-mirror plane are thought to arise from intermolecular (crystal packing) interactions, as ^{1}H NMR data indicate that the molecules adopt C_s symmetry in solution. The 1-naphtholate coligand of **4** (Figure 3) lies close to the pseudo-mirror plane, the corresponding dihedral angle being 3.1°.

The large Mo−O−C angles (>155°) in complexes **1**−**3** are consistent with considerable steric crowding at the coligand binding site. A measure of the frontal steric congestion in the dioxo-Mo(VI) complexes is provided by the relative distance of the oxo and coligand atoms from the Tp^{iPr} C(15), C(25), C(35), or C(*n*5), plane and by the Mo═O···HC$_{OAr}$ separations. For **1**, O(2) and O(3) lie 2.119(6) and 2.140(6) Å, respectively, out of the said plane. However, the *tert*-butyl carbon atoms lie an average of 5.308 Å out of the same plane; i.e., they project forward of the oxo ligands and provide steric protection to the MoO_2 unit. The Mo═O···HC contact distances between the oxo and *tert*-butyl methyl groups in **1** are ca. 2.9 Å, only marginally greater than the distance between the oxo groups and isopropyl methine hydrogens (ca. 2.5 Å). For **2**, O(2), O(3) and the *sec*-butyl carbon atoms lie 2.145(5), 2.157(5), and 5.52(1) Å, respectively, out of the C(*n*5) plane. In this case, the Mo═O···HC contact distances between the oxo and *sec*-butyl methyl groups are again ca. 2.9 Å. For **3**, the O(2), O(3), and 2-methyl carbon atoms lie 2.148(6), 2.181(6), and 2.209(3) Å out of the C(*n*5) plane, the closest Mo═O···HC contact distances being ca. 2.5 Å. The aforementioned shielding of the 6-H (at C(2) in Figure 1) or 6-CH_3 protons of **1**−**3** is consistent with the maintenance of these solid-state structures in solution. Interestingly, **4** also displays considerable frontal steric congestion in the solid state, with the C(2)−H atom located only 2.8 Å from the oxo groups, with the ligand orientation facilitated by a much smaller Mo−O−C angle of 131.5(2)°. Here, the C(4), C(5), and C(6) atoms of the naphthalene ring protrude 6.014(6), 4.913(7), and 5.096(9) Å, respectively, from the C(*n*5) plane, the oxo ligands being 2.213(3) and 2.209(3) Å from the same plane. The same degree of frontal steric congestion in the oxosulfido-Mo(VI) analogues of **1**−**4** would prevent the close approach necessary for dimerization. The corresponding oxo sulfido complexes of **1**−**3** are indeed *monomeric* in the solid state.[18]

In complexes **7**−**10** the coligand is oriented back into the proximal Tp^{iPr} cleft on the pseudo-mirror plane and the atoms projecting toward the frontal plane lie relatively close to the C(*n*5) plane. Moreover, the smaller Mo−O−C angles

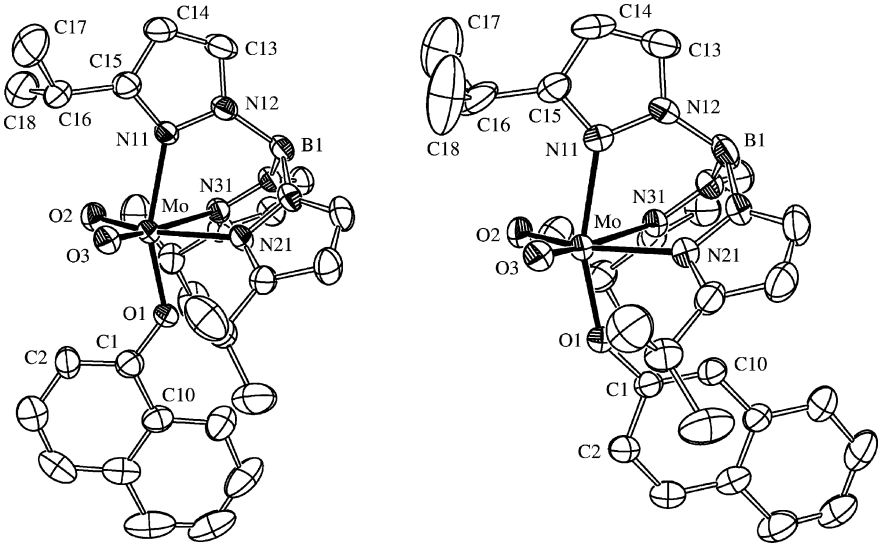

Figure 3. ORTEP projections of **4** (left) and **9** (right). Ellipsoids are drawn at the 40% and 30% probability levels, respectively, and hydrogen atoms have been removed.

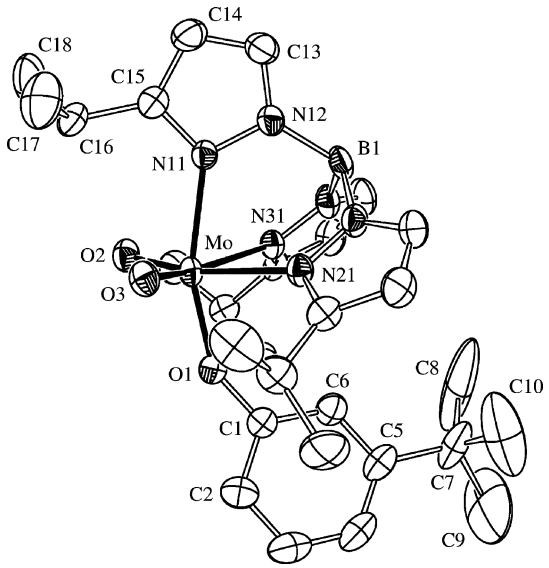

Figure 4. ORTEP projection of **7** drawn at the 30% probability level with hydrogen atoms removed.

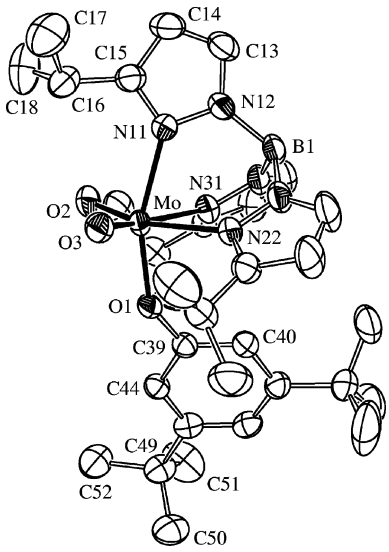

Figure 5. ORTEP projection of **8** drawn at the 40% probability level with hydrogen atoms removed.

(<150°) in **7**−**10** compared to those of **1**−**3** reflect the reduced steric demands adjacent to O(1) in the former group. Although variable, the nearest Mo═O···HC separations are all greater than 4.4 Å in **7**−**10**; the ca. 2.5 Å contacts between the oxo and isopropyl methine protons persist. In **7** (Figure 4), the 3-*tert*-butyl group is oriented toward the Tp^{iPr} cleft, directing the sterically undemanding 6-H toward the frontal region; the Mo═O···HC distance is 4.4 Å. A similar orientation is adopted by the coligand in **8** (Figure 5), with the 3-*tert*-butyl group in the Tp^{iPr} cleft and the 5-*tert*-butyl group projecting away from the oxo groups; the 6-H atom is 4.4 and 4.9 Å from the two oxo ligands. The planar arene rings make dihedral angles of 19 and 26° to the pseudo-mirror plane for **7** and **8**, respectively; these displacements from C_s symmetry are ascribed to crystal packing effects. The 2-naphtholate ligand of **9** (Figure 3) projects away from the metal center with the closest Mo═O···HC distances exceeding 4.7 Å; the naphthalene unit lies very close to the pseudo-mirror plane, the applicable dihedral angle being 3.0°. In **10** (Figure 6), the coligand biphenyl unit projects away from the oxo groups, with the phenolate ring close to the pseudo-mirror plane and twisted slightly with respect to the terminal phenyl ring. The Mo═O···HC distances are 4.6 and 4.8 Å. The observed shielding of the 2-H proton of **7** (at C(6) in Figure 4) suggests that the solid state structure is retained in solution; however, NMR spectroscopy shows only a single coligand methyl resonance for **8**, suggesting that this and the remaining complexes are fluxional in solution.

On account of their minimal frontal steric congestion, the oxosulfido-Mo(VI) complexes derived from **7**−**12** were expected to crystallize as *dimeric* disulfido-Mo(V) species. However, this was not always the case. Some derivatives, for example the oxosulfido analogue of **9**, convert into molybdenyl complexes containing bidentate O,S-donor ligands derived from the sulfido and coligand units. This transformation would be facilitated by conformationally flexible coligands.[18] Moreover, the oxosulfido analogue of **10** is

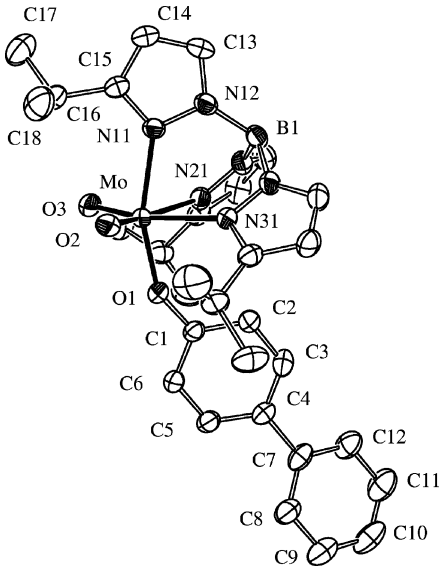

Figure 6. ORTEP projection of **10** drawn at the 40% probability level with hydrogen atoms removed.

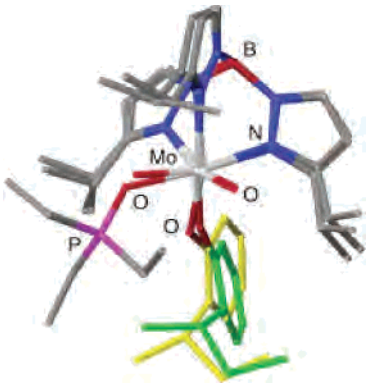

Figure 7. Superposition of Tp$^{i\mathrm{Pr}}$MoO$_2$(OC$_6$H$_4$^{s}Bu-2) (phenolate colored green) and Tp$^{i\mathrm{Pr}}$MoO(OC$_6$H$_4$^{s}Bu-2)(OPEt$_3$) (phenolate colored yellow).

monomeric in the solid state, contrary to expections based on the degree of frontal steric congestion in solid **10**. In this case, quite different conformations are adopted by the coligand in the dioxo and oxosulfido complexes.[18b]

In summary, the structural analysis of dioxo-Mo(VI) complexes provides a valuable indication of the expected nuclearity of their oxosulfido-Mo(VI) analogues. Complexes bearing 2-phenolate coligands with sustained steric congestion at the frontal O_3-donor face form monomers upon conversion to their Tp$^{i\mathrm{Pr}}$MoOS(OAr) analogues. Alternatively, oxosulfido derivatives containing sterically undemanding or conformationally flexible coligands dimerize upon crystallization, unless subsequent reactions or alternative coligand conformations prevent this.

Tp$^{i\mathrm{Pr}}$MoO(OAr)(OPEt$_3$) Complexes. Green Tp$^{i\mathrm{Pr}}$MoO(OAr)(OPEt$_3$) were synthesized by reacting Tp$^{i\mathrm{Pr}}$MoO$_2$(OAr) with PEt$_3$ in MeCN or benzene. The reaction times varied from several hours to several days, but in most cases overnight reactions provided good yields (60−85%). ^{31}P NMR monitoring of selected in situ reactions revealed reaction rates in the order **9** > **8** > **6** > **11** > **7** > **2** > **1**. These broadly correlate with the steric protection afforded the oxo ligands by the naphtholate/phenolate coligands, the 2-alkyl derivatives being the slowest to react. As described in a forthcoming paper, the conversion of Tp$^{i\mathrm{Pr}}$MoO$_2$(OPh) to Tp$^{i\mathrm{Pr}}$MoO(OPh)(OPEt$_3$) is first order in both complex and phosphine, the second-order rate constant being 7.04(6) × 10^{-2} $M^{-1}\cdot s^{-1}$; an associative mechanism is indicated by measured activation parameters.[15c] Complex **3** failed to react with available phosphines, presumably due to the steric bulk of the phenolate coligand. The products were isolated as microcrystalline solids by evaporation of the solvent and trituration or sonication of the residue in hexane. With the exception of Tp$^{i\mathrm{Pr}}$MoO(OC$_6$H$_4$^{t}Bu-2)(OPEt$_3$), which decomposed within minutes, the complexes were moderately stable (ca. 1−2 days) in air in the solid state. The preparation and properties of the oxo(phosphine oxide)-Mo(IV) complexes derived from **3**, **7**, and **8** have been reported;[15b] their chemical and spectroscopic properties parallel those described below for the title complexes.

In wet, nondeoxygenated solvents, Tp$^{i\mathrm{Pr}}$MoO(OAr)(OPEt$_3$) rapidly decomposed to their Tp$^{i\mathrm{Pr}}$MoO$_2$(OAr) counterparts; however, all species were soluble and stable in dry, deoxygenated, nonhalogenated solvents such as toluene, benzene, and, to a lesser extent, hexane. Notably, Tp$^{i\mathrm{Pr}}$MoO(OC$_6$H$_4$^{t}Bu-2)(OPEt$_3$) exhibited markedly poorer solubility characteristics than the other examples; this derivative also required extended reaction times for complete reduction of the dioxo-Mo(VI) precursor. Dissolution of the complexes in dichloromethane produced paramagnetic Tp$^{i\mathrm{Pr}}$MoOCl(OAr) via formal chlorine atom transfer.[25,26]

Microanalytical and mass spectrometric data were consistent with the proposed formulations (see Supporting Information). Infrared spectra exhibited a strong band at ca. 950 cm^{-1}, which was assigned to the ν(Mo═O) vibration of the terminal oxo ligand. Bands in the 1060−1190 cm^{-1} region were assigned to the ν(P═O) vibration of the phosphine oxide ligand; as expected, the ν(P═O) bands of the ligands were 30−100 cm^{-1} lower in energy than the band in free OPEt$_3$ (1166 cm^{-1}).[27] The presence of Tp$^{i\mathrm{Pr}}$ and phenolate ligands was confirmed by characteristic fingerprint bands (vide supra).

The ^{1}H NMR spectra of the chiral Tp$^{i\mathrm{Pr}}$MoO(OAr)(OPEt$_3$) complexes displayed resonance patterns consistent with C_1 symmetry. Notably, the isopropyl methyl and methine protons of Tp$^{i\mathrm{Pr}}$ give rise to six doublets (integrating at 3:3:3:3:3:3) and three septets (1:1:1), respectively, with the pyrazole ring methine protons yielding six doublet resonances from δ 5.8−7.8. The phosphine oxide ligand gives rise to complex resonance patterns due to the presence of diastereotopic methylene protons under C_1 symmetry. These inequivalent protons produce two doublet of doublet of quartet resonances resulting from $^2J_{PH}$, $^2J_{AB}$, and $^3J_{HH}$ couplings; the methyl groups produce a doublet of triplet resonance

(25) Roberts, S. A.; Young, C. G.; Kipke, C. A.; Cleland, W. E., Jr.; Yamanouchi, K.; Carducci, M. D.; Enemark, J. H. *Inorg. Chem.* **1990**, *29*, 3650−3656.
(26) Xiao, Z.; Bruck, M. A.; Enemark, J. H.; Young, C. G.; Wedd, A. G. *J. Biol. Inorg. Chem.* **1996**, *1*, 415−423.
(27) Hooge, F. N.; Christen, P. J. *Rec. Trav. Chim. Pay-Bas* **1958**, *77*, 911−922.

due to $^3J_{PH}$ and $^3J_{HH}$ coupling. The crystal structure of $Tp^{iPr}MoO(OC_6H_4{}^sBu\text{-}2)(OPEt_3)$ has been determined.[15b] The complex exhibits a six-coordinate, distorted octahedral geometry, with Mo═O, Mo−OAr, Mo−OP, and O═P bond distances of 1.682(2), 2.036(2), 2.168(2), and 1.511(2) Å, respectively, and obtuse O−Mo−O (O═Mo−OP = 98.08(9)° and O═Mo−OAr = 108.89(10)°) and acute N−Mo−N (average 82.1°) angles. Although the position of the phenolate coligand has shifted slightly with respect to its position in **2**, a broadly analogous conformation, conferring frontal steric protection to the metal center, persists in this, the immediate precursor to monomeric $Tp^{iPr}MoOS(OC_6H_4{}^sBu\text{-}2)$ (Figure 7). The same is true of the oxosulfido-Mo(VI) complex itself.[18] This conservation of conformation confirms that structural analysis of dioxo-Mo(VI) complexes is a valid method for estimating the steric congestion at the MoO_2S face of their oxosulfido-Mo(VI) counterparts.

Conclusion

This paper describes the synthesis, characterization, and structural analysis of $Tp^{iPr}MoO_2(OAr)$ complexes and their subsequent reaction with PEt_3 to yield $Tp^{iPr}MoO(OAr)(OPEt_3)$. The dioxo-Mo(VI) complexes complement the limited number of Tp^{iPr} complexes in the literature, and the crystal structures add significantly to the structural data available for complexes of this type. The oxo(phosphine oxide)-Mo(IV) complexes constitute rare examples of detectable/isolable intermediates in OAT from Mo(VI) to P(III).[15,28] The structural survey indicates that the 2- and 2,6-phenolates and 1-naphtholate coligands adopt conformations producing significant frontal steric congestion. This is expected to enhance strict *monomerization* in the corresponding oxosulfido-Mo(VI) complexes (as observed with 2-phenolates). Other derivatives provide less frontal steric congestion, and their oxosulfido-Mo(VI) analogues are expected to crystallize as dimers providing subsequent reactions or coligand rearrangements do not occur. Attempts to limit dimerization of oxosulfido complexes by fine-tuning redox potentials have proved less successful; e.g., the oxosulfido-Mo(VI) complex derived from **8** (with one of the most negative reduction potentials in the series) crystallizes as a dimer.[18]

Acknowledgment. We gratefully acknowledge the experimental assistance of Mr. Craig Gourlay and the financial support of the Australian Research Council and the donors of the Petroleum Research Fund (administered by the American Chemical Society).

Supporting Information Available: Full listings of analytical, mass spectrometric, and IR data for all compounds and crystallographic data in CIF format. This material is available free of charge via the Internet at http://pubs.acs.org.

IC050052V

(28) (a) Nemykin, V. N.; Davis, S. R.; Mondal. S.; Rubie, N.; Kirk, M. L.; Somogyi, A.; Basu, P *J. Am. Chem. Soc.* **2002**, *124*, 756−757. (b) Nemykin, V. N.; Laskin, J.; Basu, P. *J. Am. Chem. Soc.* **2004**, *126*, 8604−8605. (c) Nemykin, V. N.; Basu, P. *J. Chem. Soc., Dalton Trans.* **2004**, 1928−1933.